Supplement of Earth Syst. Sci. Data, 17, 3741–3756, 2025
https://doi.org/10.5194/essd-17-3741-2025-supplement


Open Access Earth System Science Data

*Supplement of*

# Global high-resolution fire-sourced $PM_{2.5}$ concentrations for 2000–2023

**Yonghang Hu et al.**

*Correspondence to:* Xu Yue (yuexu@nuist.edu.cn)

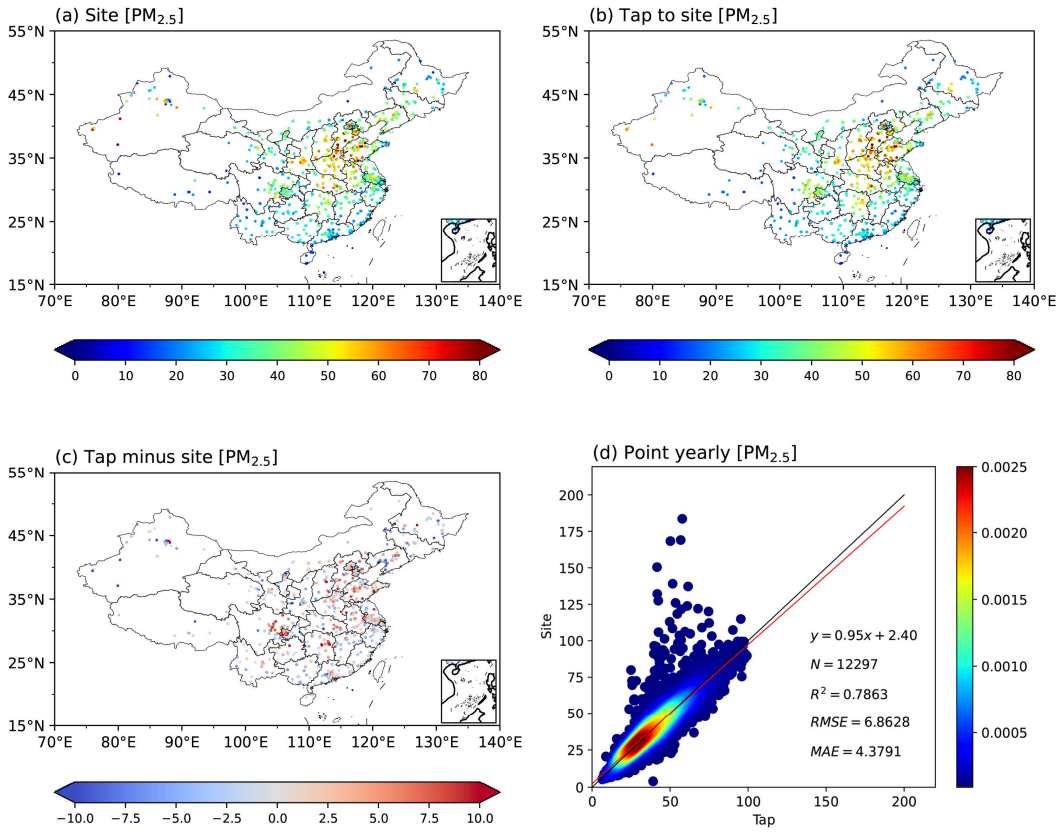


**Figure S1.** Comparison of observed and interpolated $PM_{2.5}$ concentrations ([$PM_{2.5}$]) in China from 2015 to 2022. Panel (a) displays annual mean [$PM_{2.5}$] (μg $m^{-3}$) at 1822 monitoring sites. Panel (b) shows interpolated annual mean [$PM_{2.5}$] from Tracking Air Pollution (TAP) dataset. Panel (c) presents the difference between interpolated and observed values. Panel (d) compares annual mean [$PM_{2.5}$] at each site with observations, with colors indicating data frequency. Validation metrics, including sample size (N), regression equation, determination coefficient ($R^2$), root-mean-square error (RMSE), and mean absolute error (MAE) are also provided.

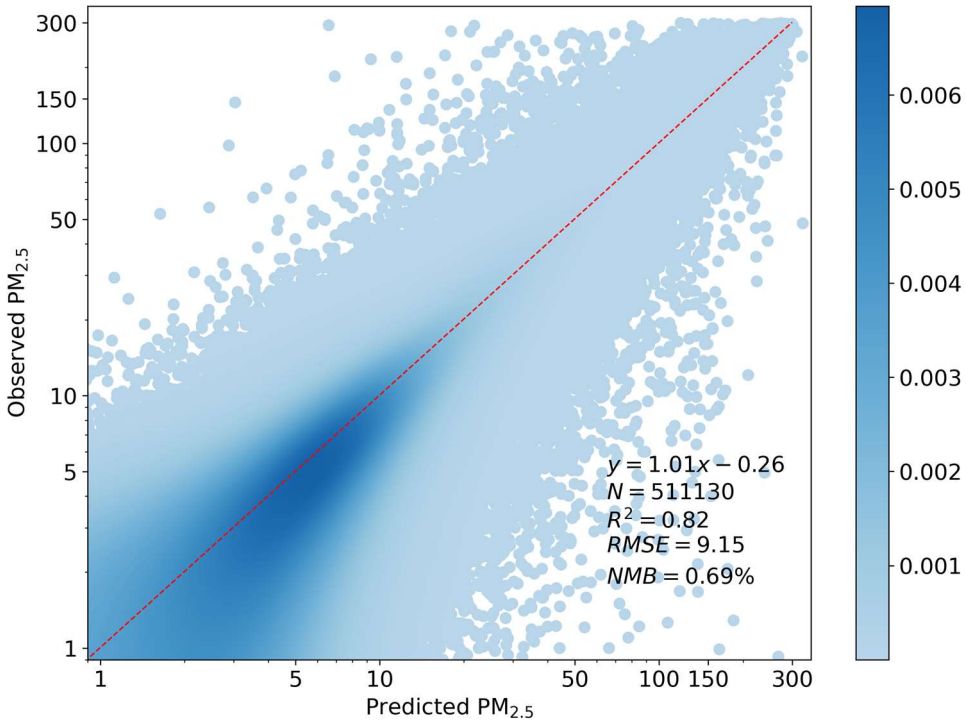


**Figure S2.** Same as Fig. 1b, but for GEOS-Chem simulations using the QFED inventory.

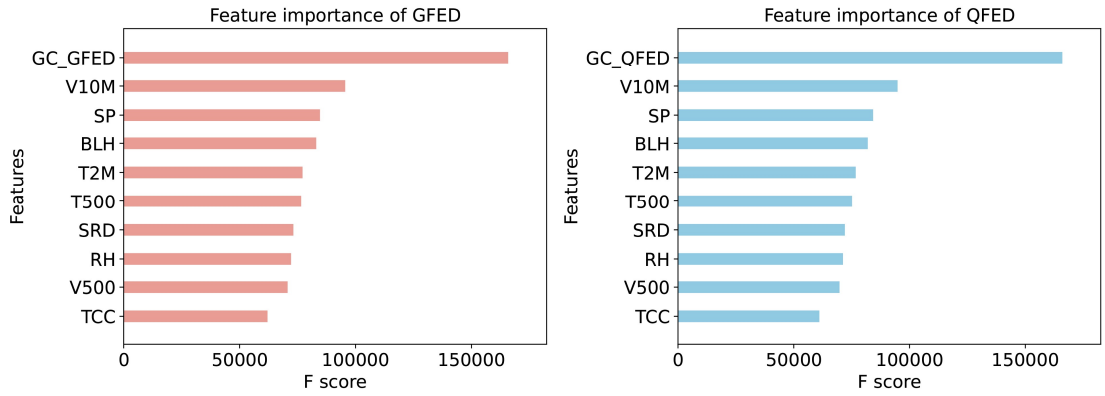


**Figure S3.** Top 10 important features measured by F-score for the machine learning model, which was trained using GEOS-Chem simulations with fire emissions from (a) GFED and (b) QFED inventories in 2022, respectively. The full name of each feature is shown in Table S1.

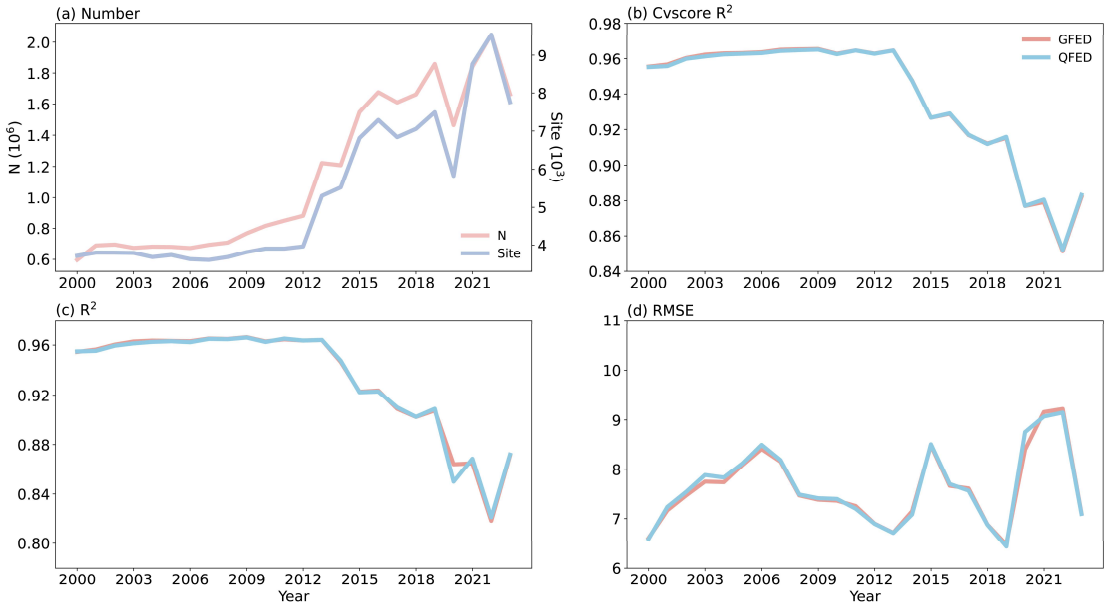


**Figure S4.** Statistical metrics of estimated [$PM_{2.5}$] from 2000 to 2023. Panel (a) shows the total number of sites and samples (N) used for machine learning training. Panel (b) presents the 10-fold cross-validation $R^2$ for each year, comparing estimations using different fire emission inventories, including GFED and QFED. Panels (c) and (d) display the year-to-year $R^2$ and RMSE between observed and estimated [$PM_{2.5}$] using these different fire emission inventories for independent validation samples.

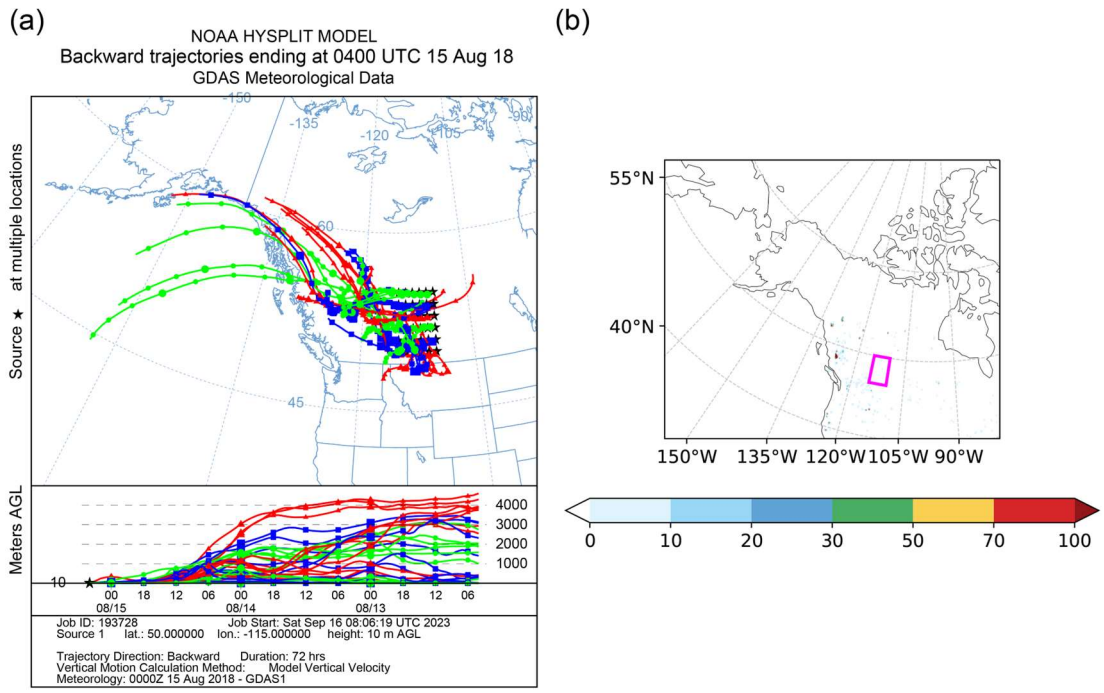


**Figure S5.** The 72-hour backward trajectories of Canadian sites ending on August 15$^{th}$, 2018, generated using the NOAA HYSPLIT Trajectory Model. The horizontal and vertical trajectories are shown in (a) and the fire emissions of GFED inventory (units: g m$^{-2}$ yr$^{-1}$) averaged for August 13-15, 2018 are shown in (b). The pink box represents the range of sites in Canada.

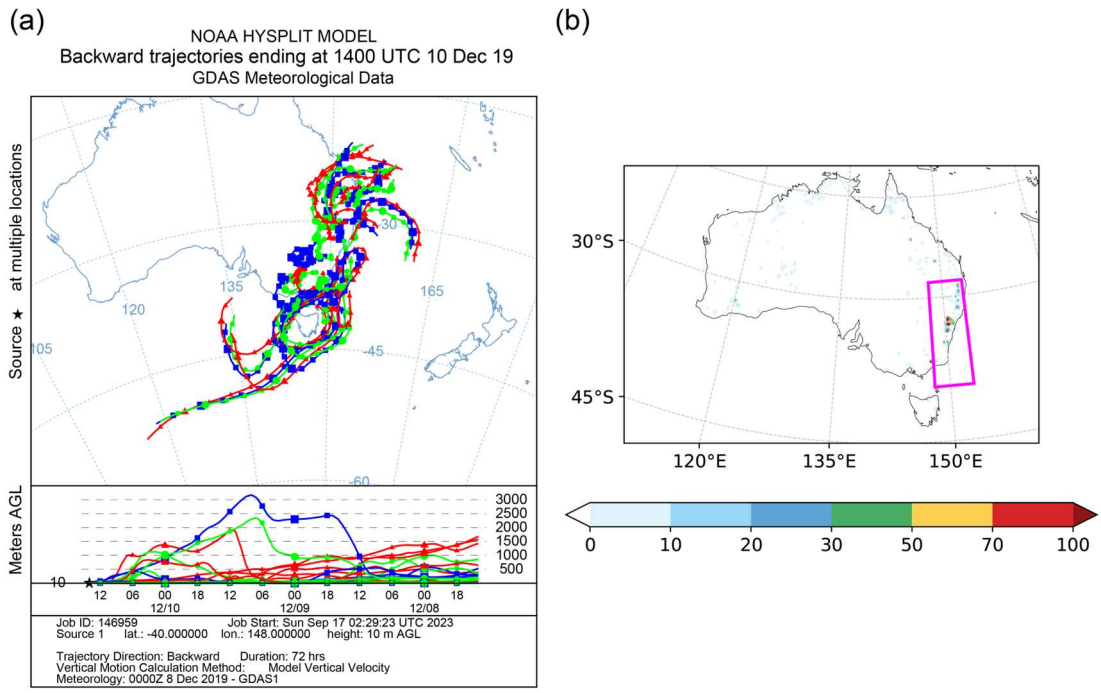


**Figure S6.** The same as Fig. S5 but for the backward trajectories of Australian sites ending on December 10$^{th}$, 2019.

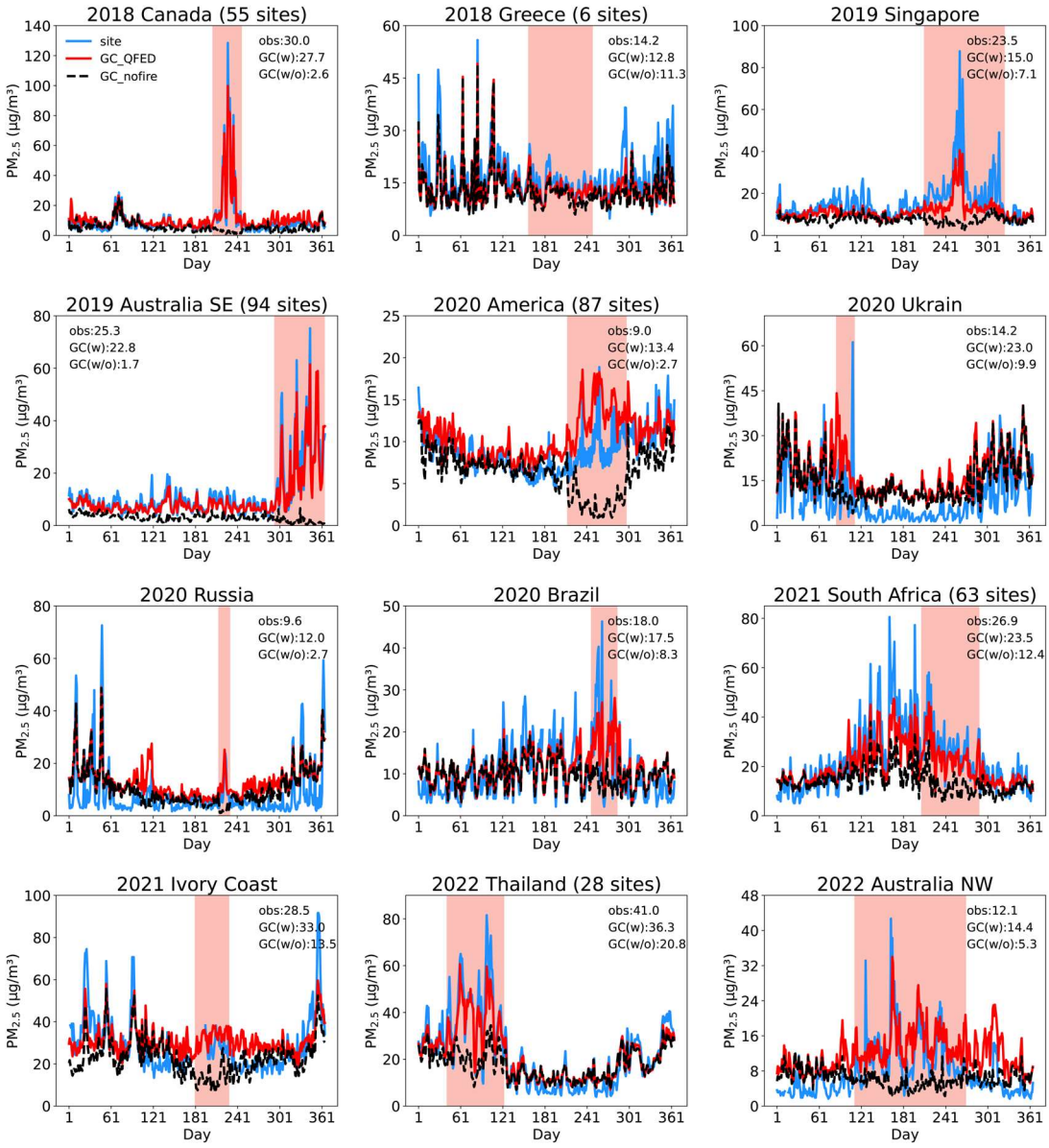


**Figure S7.** The same as Fig. 3 but the estimated [$PM_{2.5}$] is derived using QFED fire emission inventory.

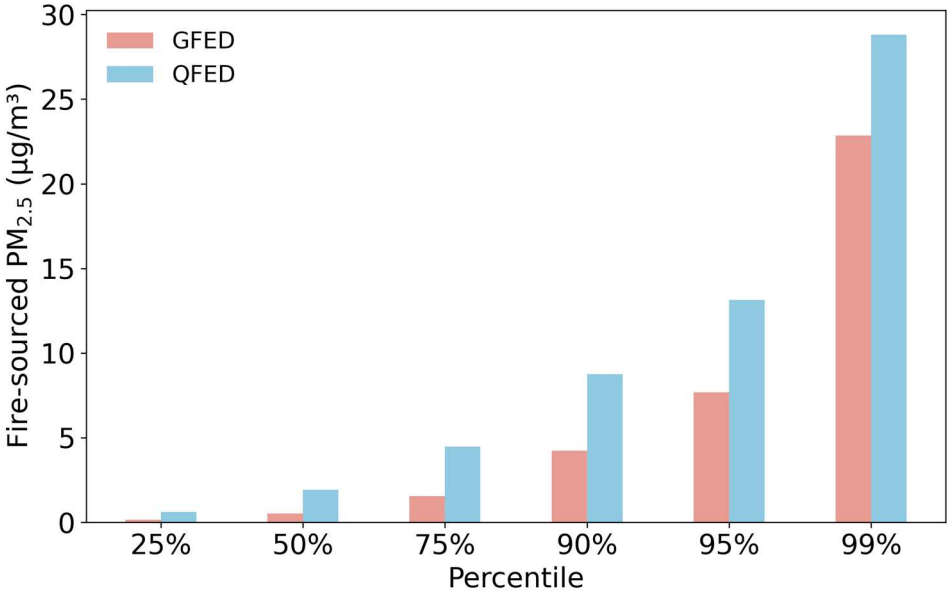


**Figure S8.** Comparison of daily fire-sourced [$PM_{2.5}$] at different percentiles between simulations with GFED and QFED inventories.

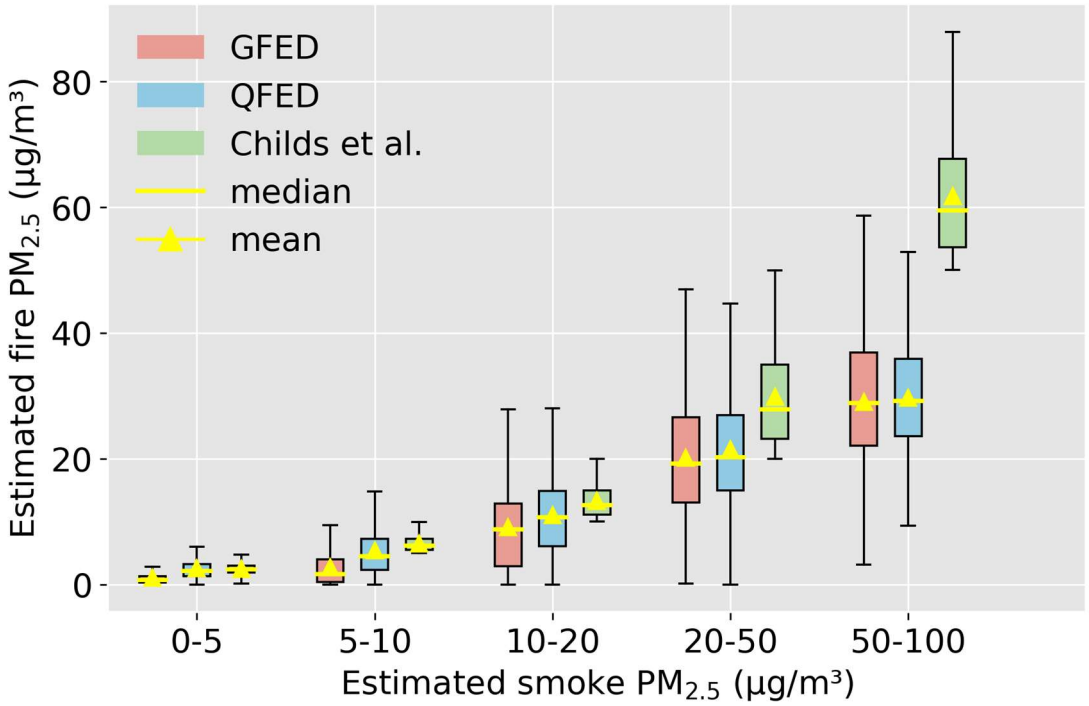


**Figure S9.** Boxplot of estimated GFED and QFED fire $PM_{2.5}$ v.s. Childs et al. (2022) estimated smoke $PM_{2.5}$ under various levels.

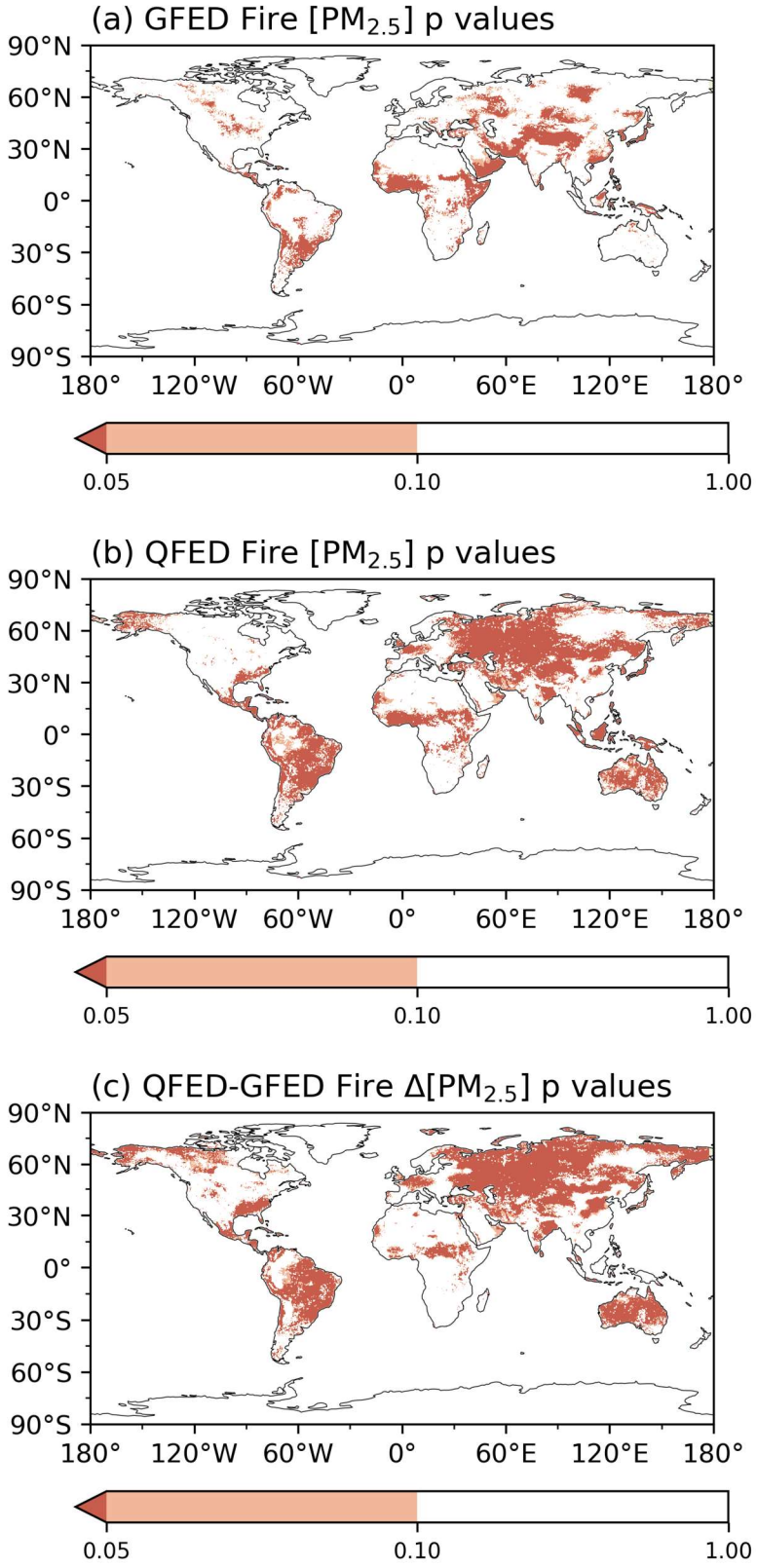


**Figure S10.** The *p* values of long-term (a) trends in fire [$PM_{2.5}$] derived using the GFED inventory for 2000-2023. Panels (b) and (c) display the same information as (a), but for fire [$PM_{2.5}$] from QFED inventory and differences between QFED and GFED inventories.

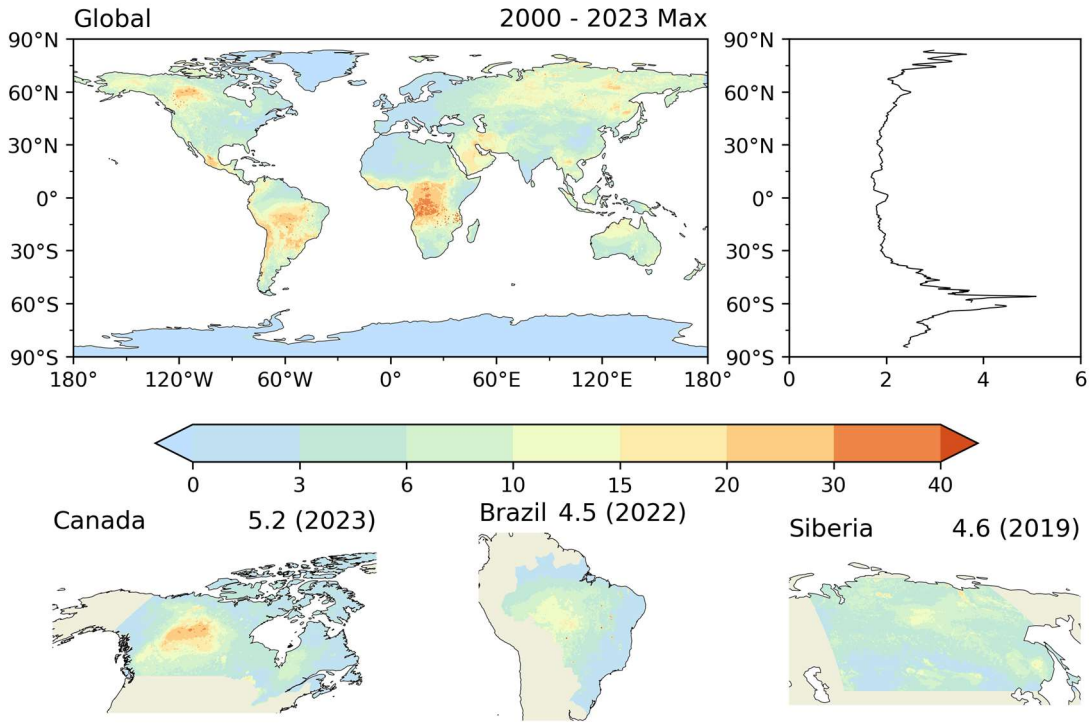


**Figure S11.** The same as Fig. 7 but with fire emissions from the QFED inventory.

**Table S1** Summary of the input for machine learning model

| Variables | Descriptions |
|---|---|
| GC_GFED | Simulated [$PM_{2.5}$] by GEOS-Chem using GFED emissions |
| GC_QFED | Simulated [$PM_{2.5}$] by GEOS-Chem using QFED emissions |
| BLH | Boundary layer height |
| Pc | Convective precipitation |
| Pls | Large scale precipitation |
| Pt | Total precipitation |
| T2M | 2m temperature |
| T2X | Maximum 2m temperature since previous post processing |
| T2N | Minimum 2m temperature since previous post processing |
| RH | Relative humidity |
| SP | Surface pressure |
| SRD | Surface solar radiation downwards |
| T500 | Temperature 500hPa |
| T850 | Temperature 850hPa |
| TCC | Total cloud cover |
| V10M | Wind speed at 10m |
| V500 | Wind speed at 500hpa |
| V850 | Wind speed at 850hpa |
| F_Water | The cover fraction of Water |
| F_ENF | The cover fraction of Evergreen Needleleaf Forest |
| F_EBF | The cover fraction of Evergreen Broadleaf Forest |
| F_DNF | The cover fraction of Deciduous Needleleaf Forest |
| F_DBF | The cover fraction of Deciduous Broadleaf Forest |
| F_Mforest | The cover fraction of Mixed Forests |
| F_Cshrub | The cover fraction of Closed Shrubland |
| F_Oshrub | The cover fraction of Open Shrubland |
| F_Wsavanna | The cover fraction of Woody Savannas |
| F_savanna | The cover fraction of Savannas |
| F_grass | The cover fraction of Grasslands |
| F_Pwetland | The cover fraction of Permanent Wetlands |
| F_crop | The cover fraction of Croplands |
| F_urban | The cover fraction of Urban and Built-up |
| F_CVM | The cover fraction of Cropland/Natural Vegetation Mosaic |
| F_snow | The cover fraction of Snow and Ice |
| F_barren | The cover fraction of Barren or Sparsely Vegetated |

**Table S2** Spatiotemporal information of wildfire episodes

| Event | Region | Time |
|---|---|---|
| 2018 Canada | British Columbia | 2018.7-2018.8 |
| 2018 Greece | Athens | 2018.6-2018.8 |
| 2019 Singapore | Sumatra | 2019.8-2019.11 |
| 2019 Australia SE | New South Wales | 2019.10-2019.12 |
| 2020 Ukrain | Chernobyl | 2020.3-2020.4 |
| 2020 Russia | Siberia | 2020.8 |
| 2020 Brazil | Sao Paulo | 2020.9-2020.10 |
| 2021 Ivory Coast | Yamoussoukro | 2021.7-2021.9 |
| 2021 South Africa | Limpopo | 2021.7-2021.10 |
| 2022 Australia NW | Northern Territory | 2022.4-2022.9 |
| 2022 Thailand | Lampang | 2022.4-2022.5 |